International Journal of Science and Technology (IJST)
ISSN: 3049-1118, Volume- 2, Issue- 2 (Apr – Jun 2025)

Novel Synthesis and Fabrication of CuO/RGO Composite Modified Electrode for Selective Electrochemical Determination of Environmental Pollutant Para-Aminophenol in Water and Fruit Sample

Palpandi karuppaiah*
ORCID ID: 0009-0003-2698-3455

Abstract

Carbon-based nanomaterials such as graphite and their oxides have attracted extensive attention in many areas, especially in organic synthesis, electrochemistry, and catalytic chemistry. In this context, we report new eco-friendly preparation of copper oxide/reduced graphene oxide nanocomposites (CuO/RGO) based para-Aminophenol (PAP) electrochemical sensor. The synthesized nanocomposites was characterized by X-ray diffractometer (XRD), Fourier transform infrared spectroscopy (FTIR), Energy dispersive X-ray spectrometry (EDS) and field emission scanning electron microscope study (FESEM). The electro catalytic behavior of PAP at the surface of CuO/RGO nanocomposite on screen-printed carbon electrode (SPCE) was investigated in detail. Combining CuO and RGO intensifies the property and performance of the nanocomposites Due to coactive effects between RGO nanosheets and CuO nanoparticles. Herein, PAP is used as a probe to appraise the electro catalytic activities of the CuO/RGO modified electrode. In this study, we were able to obtain a detection limit (LOD) of 0.02µM and a wide linear concentration ranging (LR) from 0.01µM to 478.1µM for PAP. The nanocomposites exhibits excellent and stable electro catalytic activity for the PAP determination.

Keywords: Environmental pollutants, para-Aminophenol, metal oxide-graphene nano-hybrid, Cyclic voltammetry, impedance spectroscopy.

1. Introduction

Aminophenol and its chemical derivatives are ubiquitous in the terrain and substantially come from the plant disposals Due to their use in the production of pharmaceutical products as an intermediate form, ménage particulars, explosive substances, and in leather processing diligence. These chemicals have the eventuality to ply dangerous goods on mortal beings, cattle, and shops; indeed in its smallest attention [1-4]. Further than 165 phenolic's are well-known to have an adverse effect on the terrain. These chemicals, besides their vapour, are largely sharp to eyes, skin, and respiratory organs. Due to phenolic's acidulous and ante-adipose goods, dragged exposure to skin can beget dermatitis or indeed alternate and third-degree becks. They're also do dangerous goods on the central nervous system (CNS), and heart, causing dysrhythmia, seizures,

* Corresponding Author Email: sensorpandian18@gmail.com
Published: 26/06/2025

coma, and order trauma [5]. The United States Environmental Protection Agency (EPA) has listed 1mg/L^1 as the limit for exposure to all general phenolic combinations [6], and the European Community [EC] directive specifies the legal permissible position of 0.5 mg/ L^1 for phenolic composites for mortal application [7]. Para-aminophenol (PAP) is extensively used as a precursor in the product of antipyretic analgesic medicines like acetaminophen as well as for multitudinous classes of colourings. It's also used for the medication of stabilizers in polymer accoutrements similar as 4-hydroxy-diphenyl amine, N,N'-diphenyl-1,4-phenylenediamine, and N-(4-hydroxyphenyl)-2-naphthylamines. Likewise, PAP is used in making the photographic inventor N- methyl- p- aminophenol [8]. The PAP has the double poisonous capability for both aniline and phenol. Where, immersion of it through the skin can cause dermatitis as well as methemoglobinemia, and asthma. The sensitive determination and evaluation of PAP are of essential significance Due to its uninterrupted presence in the natural terrain and food substances [9].

Graphene (GR) is the most extensively analysed material and is widely exploited in various fields. Basically, it is a flat single-layer thick carbon element closely bounded onto a two-dimensional material honeycomb crystal trellis structure which is held together by a backbone of overlapping sp^2 hybridization bonds. GR is the principal component for graphitic materials of all other dimensions. These carbon atoms are arranged together by a weak van der Waals force to form graphite. Due to their astonishing characteristics such as superior electrical conductance, impermeable, excellent ocular transparency, flexibility, and very strong under tension, it has been a subject to extensive research for various applications. GR is incredibly stronger than metallic steel (~200) [10]. The wide ranging of potential applications of GR in the manufacture of electronics [11], composite materials [12], solar cell panels [13], gas sensors [14], drug delivery systems [15], and super capacitors [16]. GR can be prepared by various methods such as mechanical exfoliation [9], chemical reduction of exfoliated graphene oxide [17], chemical syntheses [18], Liquid phase exfoliation (LPE) [19], and chemical vapour deposition (CVD) [20]. Various types of metals, metal oxides, magnetic and semiconducting nanostructures involving Palladium [21], Platinum [22], Gold [23], Titanium dioxide [24], and Iron oxide [25] have been used to modify the RGO surface. Nanoparticles behave as spacers between RGO nanosheets to decrease the cluster formation and it also resists the assembly of these active Nano blocks with vast interfacial energy. These nanocomposites often exhibit the enhanced properties and improved functionalities as a result of the combined effects between RGO nanosheets, and the nanoparticles [26-27], and these hybrid nanocomposites are used as electro catalysts.

When compared with noble metallic oxide nanoparticles such as ZnO, TiO2, Fe3O4, etc., CuO is the low-cost alternative with a broad potential candidate for many applications [28-29]. The band gap energy of CuO is 1.2eV and it is categorized into a p-type semiconductor [30-31]. It has been used an antioxidant and antibacterial agents [32], photo-electrochemical water splitting [33], electrochemical dopamine sensor [34], electro-catalysts [35, 64], methane dissolution from water [36], appliances in lithium-ion batteries [37], gas sensor fabricating device [38] and photo catalyst and electrochemical paracetamol sensor [63, 65]. Zhao et al, have prepared CuO/Graphene nanostructures via hydrothermal approach in the presence of ammonia solution for super-capacitor fabrication purpose [39]. CuO/GR nanocomposites are

also exposed to improved capacity and retention ability as anode materials in lithium-ion batteries [40-42].

In this study, we present a simple method to incorporate copper oxide nanoparticles onto the RGO surface by sono-chemical approach. The resulting nanocomposites exhibits distinctive electro catalytic activity for the electrochemical reduction of PAP. The developed technique here leads to various applications and possibilities in the fabrication of RGO enriched with nanoparticles.

Observational techniques

2.1. Reagents and chemicals

Pure graphite powder, sodium nitrate ($NaNO_3$), potassium permanganate ($KMnO_4$), H_2O_2 (50% v/v), copper sulphate pentahydrate ($CuSO_4.5H_2O$), 4-aminophenol, L-ascorbic acid, sulphuric acid (98%), HCl, glucose, 4-nitrophenol, chloramphenicol, disodium sulphide, paracetamol, amoxicillin, tyrosine, uric acid, salicylic acid, were purchased from Sigma Aldrich (India).

2.2. Synthesis of CuO

In this typical procedure, we prepared the copper oxide nanostructures through sono-chemical approach by using $CuSO_4.5H_2O$ as a starting tertiary material. About 2.0gm of $CuSO_4.5H_2O$ is poured into a volumetric flask and dissolved in double distilled water and made up to 100 mL. Then, the solution is transferred to a round-bottom flask and ultrasonicated for two hours followed by dropwise addition of 2.0 gm of 100 mL alkaline solution (NaOH). At the end of the reaction, the products were collected through filtration and washed with ethyl alcohol (75%) and distilled water in order to eliminate the scum. The product was dried at 50˚C for 6 h and calcined at 400˚C for 2 h. The chemical reactions can be summarized as the following equations (1) and (2),

$$CuSO_4\ (aq) + NaOH\ (aq) \rightarrow Cu\ (OH)_2\ (solid) + Na_2SO_4\ (aq) \rightarrow (1)$$

$$Cu\ (OH)_2\ (solid) \rightarrow CuO\ (solid) + H_2O \rightarrow (2)$$

2.3. Preparation of graphene oxide and RGO

Graphene oxide (GO) were synthesized by modified Hummer's method with a slight modification [43]. In this process, L-ascorbic acid is used as the reducing agent. In a typical reduction, GO (1.0 gr) was poured into the 500 mL double distilled water in a flask and dispersed finely by ultrasonication treatment for 3 h. Thereupon, while the GO suspensions were stirred with ascorbic acid (1.0 gr) and the suspension was heated at 95-98˚C for 1 h. RGO's were precipitated by centrifugation. Afterward, the obtained RGO samples were washed firmly with ethanol and pure water thrice. Finally, the collected RGO's were dried in a vacuum dryer for 24 h at 55˚C).

2.4. Preparation of CuO/RGO nanocomposites

The nanocomposites were prepared by sono-chemical method of RGO and CuO nanoparticles. The sonication process was conducted by the use of a probe-type ultrasonic

wave generator. 20 mg of RGO was dispersed in 30.0 mL distilled water and 30 mg of CuO in 50 mL distilled water and both the solutions were separately ultrasonicated to form a homogeneous suspension. Later on, the RGO suspension was added slowly into CuO solution. Then, the mixtures were probe-sonicated for 2 h (005 rpm, Model-CML-04). Finally, the suspension was stirred with the help of magnetic stirrer at 70˚C and a black colour product was obtained after washing three times with double distilled water. The final products were dried at 85˚C for 1 h to obtain the desired CuO/RGO composite and used for further characterization. Scheme 1 illustrates the preparation of nanocomposites.

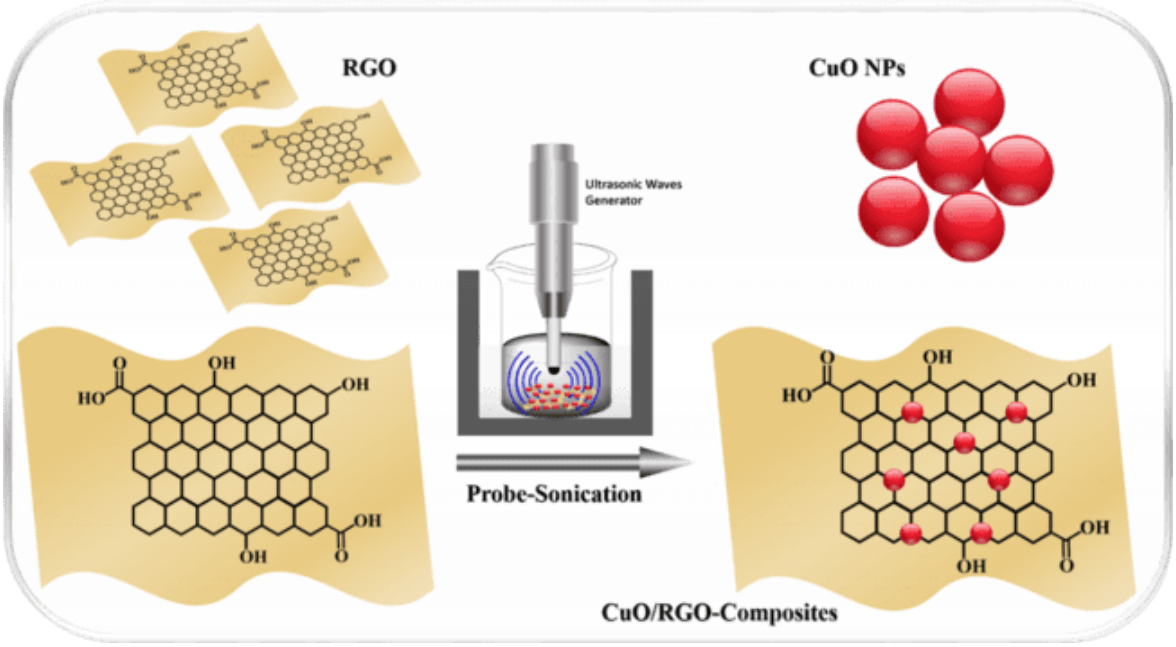

Scheme 1. Synthesis process of CuO/RGO nanocomposites.

2.5. Fabrication of CuO/RGO modified electrode for PAP determination

The PAP sensor was fabricated by drop casting CuO/RGO nanocomposites onto screen printed carbon electrode. The nanocomposites was re-dispersed in Millipore water (5mg/L^{1}) and sonicated for 1 h to obtain a uniform suspension. About 7 µL suspension was dropped on the surface of SPCE and dried at 55˚C in an oven for a few minutes. All the electrochemical analyses were carried out in ambient temperature in the presence of nitrogen. The overall process carried out in the electrochemical sensor construction is described in **Scheme 2**.

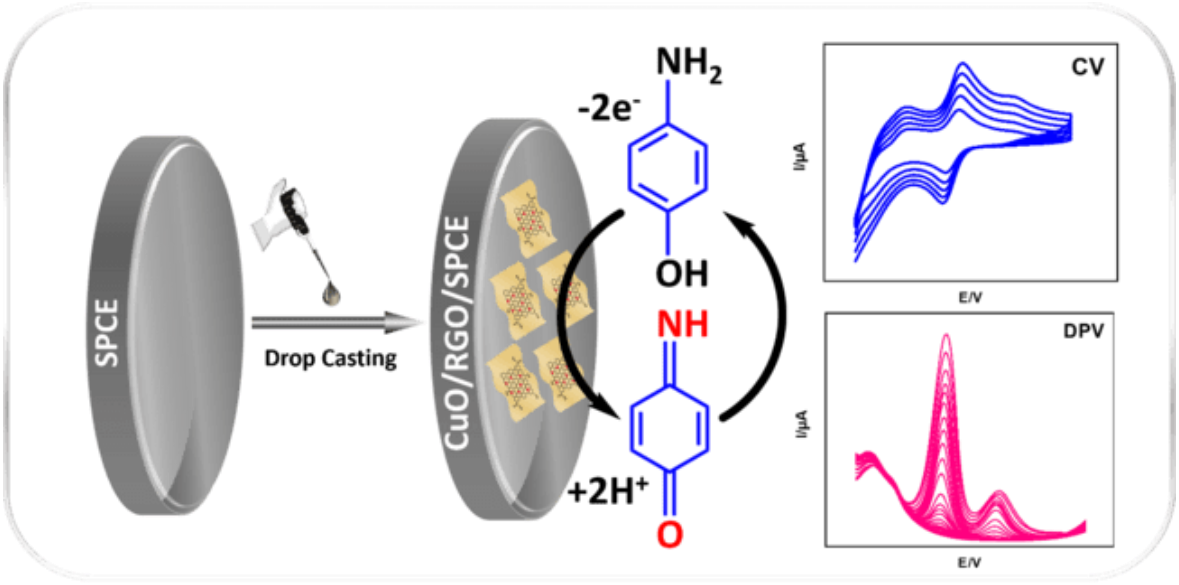

Scheme 2. The overall process of PAP determination.

1.6.Preparation of the real samples and lab sample

1.7.Lab sample

10mM of para-aminophenol was prepared in a 50 mL volumetric flask and shaken vigorously using a vortex for a few minutes. The prepared analyte was kept in the refrigerator at 4˚C when not in use. The analyte was prepared 10min before the experiment.

1.8.Real samples (river water and drinking water)

The river water sample was collected from nearest place and the drinking water was received from campus store and filtered by using a suction pump with 0.02 mm filter paper. The known concentrations of para-aminophenol were spiked into the water samples then transferred to the 25 mL of volumetric flask and stored in the refrigerator at 4˚C.

1.9.Fruit extract sample (Wild berry)

The wild berry fruit was obtained from nearest market and it Is extracted and filtered. The known concentrations of para-aminophenol were spiked into the fruit extract then transferred to the 25 mL of volumetric flask and stored in the refrigerator at 4˚C before the experiment.

Instrumentation techniques

The FTIR spectra were recorded with the samples on potassium bromide over a frequency ranging from 4000 to 400 cm^{-1} in the Nicolet model impact 410 FT-IR spectrophotometer. The morphological properties of CuO/RGO composite were characterized by field emission scanning electronic microscope (Model: JSM- 6390LV Joel, Japan) attached with energy dispersive X-ray detector. Scanning was done at micrometre ranging, and all the images were taken at an accelerating voltage between 15-20 kV with the magnifications of 15, 000x to 65, 0000x. The X-ray diffraction analysis was executed at room temperature (ca. 298 K) utilizing the Rigaku X-ray diffractometer with Cu-Ka radiation (λ = 0.154 nm) at 30 kV and 15 mA applying the scanning time of 0.05 sec-1 in the ranging of 2 Theta = (10 to 70°).

2. Results and discussion

4.1. Characterization of CuO/RGO nanocomposites

The XRD were employed to determine the position, grain size, and crystalline phase of the synthesized GO, RGO, CuO, and CuO/RGO nanocomposites. As shown in Fig. 1(A), is the diffraction peak displayed at 2θ =12.73° correspond to GO. Fig. 1(B) reveals the presence of the pronounced diffraction peaks of 2θ degrees at 26.11° point out the reduction of GO and verify the presence of RGO. Fig. 1(C) depicts the formation of CuO. According to the JCPDS card: 048-1548 all the diffractions were well matched and confirms the monoclinic phase of CuO nanoparticles. The diffraction peaks with 2θ 35.45°, 38.81°, 48.77°, and 61.47° respectively indexed to the (002)/ ($\bar{1}$11), (200), ($\bar{2}$02), (020) and (202) reflection planes. Fig.1 (D) illustrates the XRD spectrum of CuO/RGO, which exhibits the peak positions at 2θ 23.38° (002), 32.43° (110), 35.43° ($\bar{1}$11), 38.63° (111), 42.48° (100), 48.88° ($\bar{2}$02), 53.36° (020), 58.06° (202), 61.47° ($\bar{1}$13), and 66.40° (220). The average crystallite size of the CuO/RGO nanocomposites were calculated by Scherer equation (3) as follows [44],

$$X_s = k\lambda|\beta\cos\theta \qquad \rightarrow (3)$$

Here, X_s is the crystallite size, λ is the wavelength of X-ray, ß is the full width at half maximum (FWHM) of the diffraction peak, $\boldsymbol{\theta}$ is the angle of diffraction and the Scherer's constant is k. The crystallite size were computed from the diffraction plane and it was found that the crystallite size is 14.8 nm.

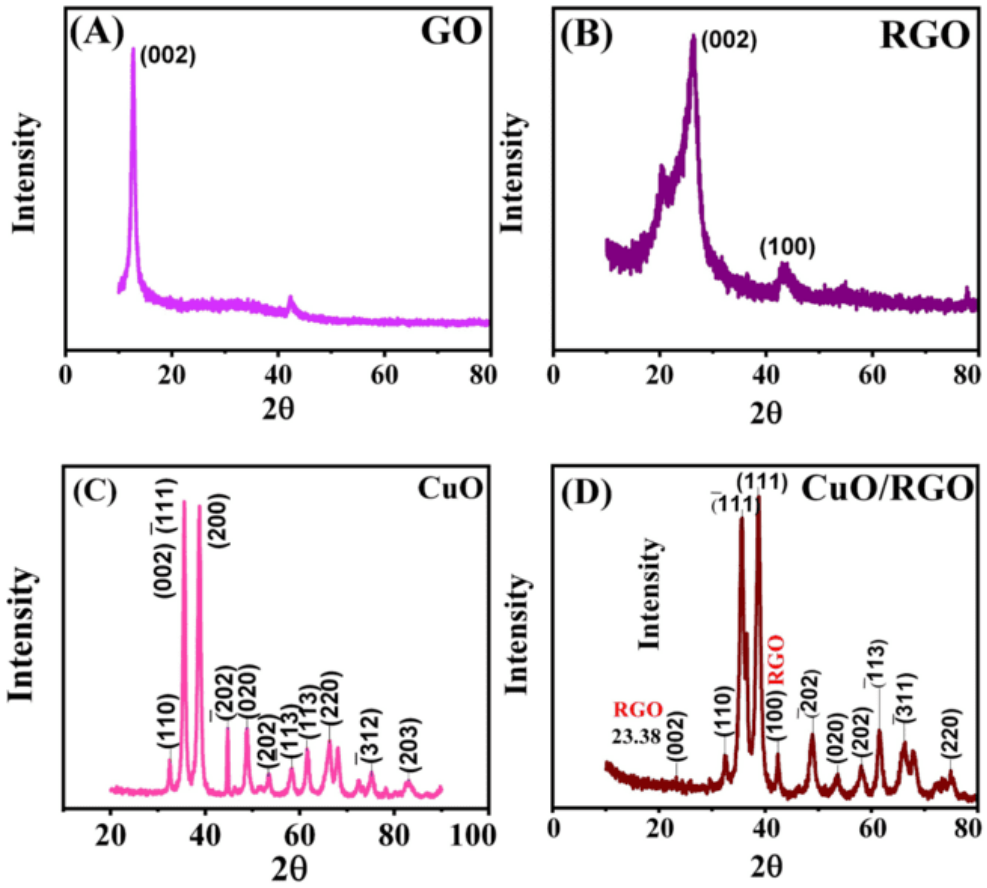

Fig.1. X-ray diffractograms of the synthesized graphene oxide (A), Reduced graphene oxide (B), Copper oxide (C), and Copper oxide/Reduced graphene oxide nanocomposites (D).

FTIR spectroscopy were used to determine the functional group of as-synthesized graphene oxide, RGO, CuO, and CuO/RGO nanocomposites. The spectra for GO reveals the absorption peaks at 3424.76, 1636.45, and 1132.69 cm^{-1} Due to the presence of hydroxyl, carboxyl and epoxy functionalities Fig. 2 (A). The progression of reduced GO peak referred to the reduction of oxygen-containing group on GO by ascorbic acid. The obtained peaks were confirmed by the removal and reduction of the intensity of the peaks. The peaks in the FTIR spectrogram at 1137.10, 1393.56 and 1661.63, 3433.96 cm^{-1} disappeared and decreased dramatically, suggesting the elimination of O_2, the functional group in the GO. The RGO spectral data shows that the most of the oxygen consisting functional group in the GO was eliminated although some residual oxygen-functionalities on GO still present in the RGO surface with weaker intensity after the reduction by ascorbic acid. The peak at 1661.36 cm^{-1} in RGO shows a strong band, suggesting the recovery of the sp^2 lattice in Fig. 2 (B). In the FTIR spectrum for CuO in Fig. 2 (C), peaks at 483.06 cm^{-1} and 1108.26 cm^{-1} correspond to strong Cu-O stretching vibration. The peak at 1710.81 cm^{-1} correspond to C=O stretching acidic group. Bands at 3311.36 cm^{-1} it could be ascribed to the Cu–OH group. In Fig.2 (D), depicting the CuO/RGO nanocomposites the intensity peak of C-O, C-OH, and C-O group reduces significantly, illustrating the GO reduction. Again, several new peaks appeared at 841.89 cm^{-1} resembling the Cu-O stretching vibration. The absorption band at 3444.26 cm^{-1}coincides with the O-H stretching vibration. These reported data confirm the formation of CuO/RGO by the sono-chemical method.

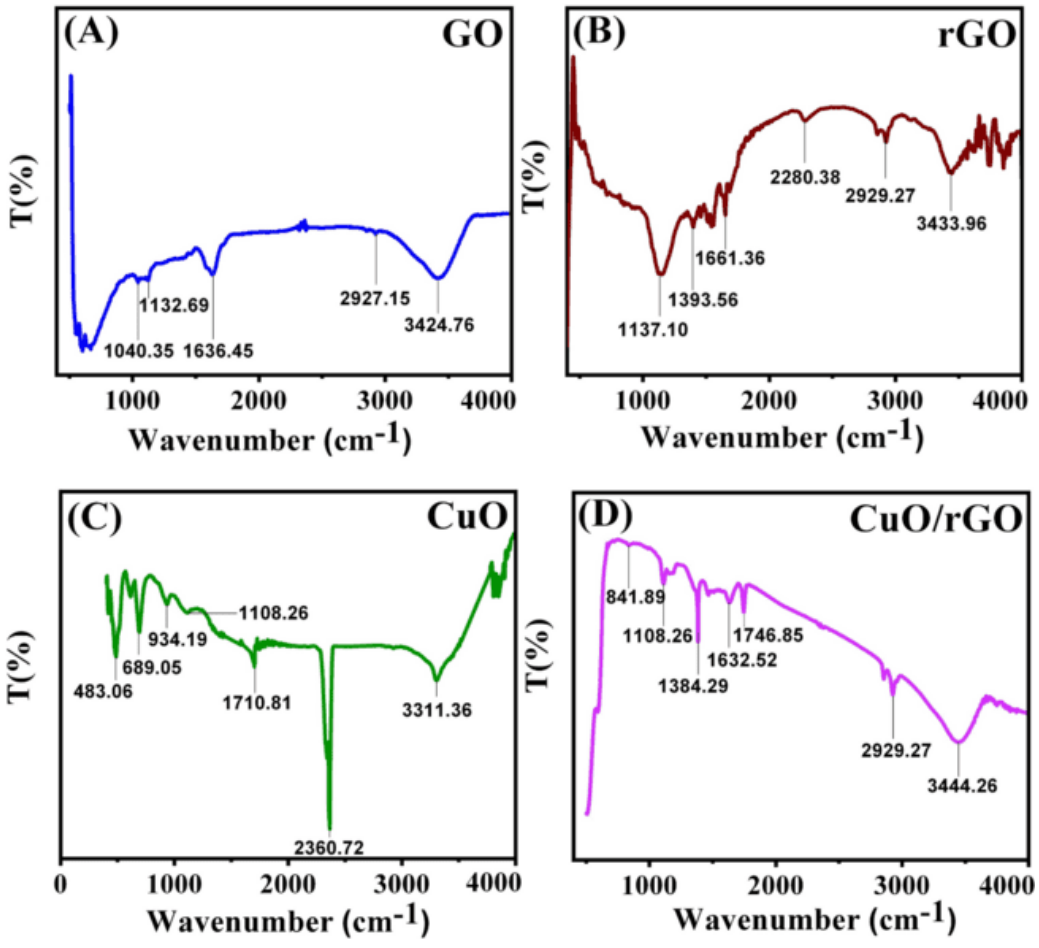

Fig. 2. Fourier-transform infrared spectroscopic analysis of GO (A), rGO (B), CuO (C) and CuO/RGO nanocomposites (D).

4.2. FESEM morphology and EDX

The surface morphological properties of the prepared GO, RGO, CuO and CuO/RGO nanocomposites was probed by the FESEM. Fig. 3 (A-B), shows the typical wrinkled sheet-like morphology of GO and RGO respectively. Fig. 3 (C) reveals the sponge-like morphology of CuO nanoparticles. The FESEM of CuO/RGO suggested that the metal oxide nanoparticles are equally spread over the wrinkled RGO surface confirming the incorporation of CuO nanoparticles onto RGO as in Fig. 3 (D).

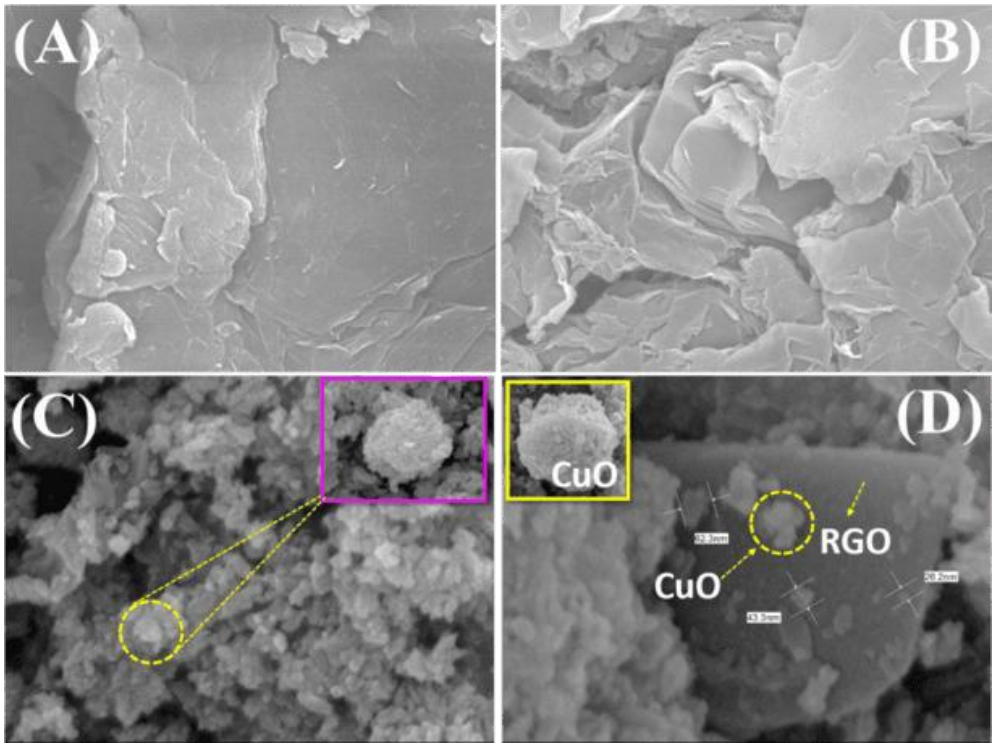

Fig. 3. FESEM morphographs of as prepared (A) GO, (B) RGO, (C) CuO and (D) CuO/RGO nanocomposites.

Energy dispersive X-ray spectroscopy was used to determine the weight percentage, elemental identification, and quantitative compositional information about the formation of CuO/RGO nanocomposites in Fig.4 (A) and the corresponding atomic weight percentages of carbon, copper, and oxygen presented in the Fig.4 (B).

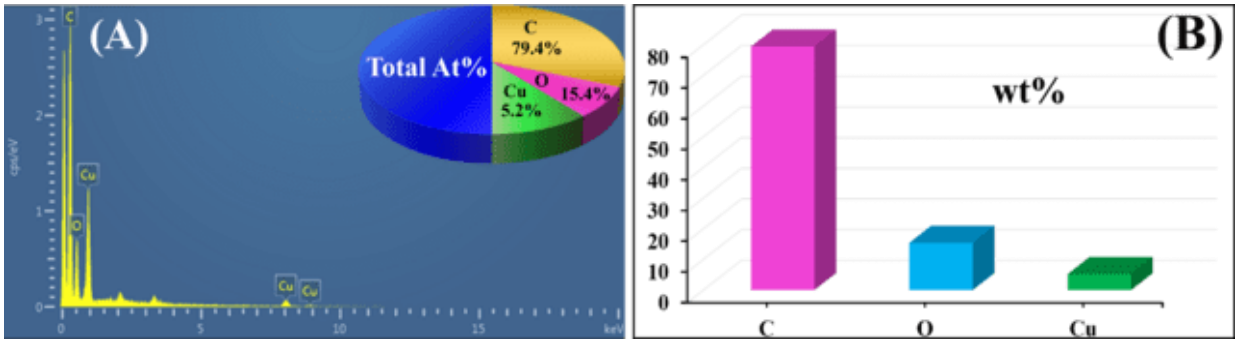

Fig. 4. EDS confirmation of CuO/RGO nanocomposites

To evaluate the locations of carbon, oxygen, and copper, elemental mapping of the CuO/RGO nanocomposites was also conducted. The obtained results are illustrated in Fig.5 (A) and Fig.5 (C-D) provide information about carbon, oxygen, and copper respectively.

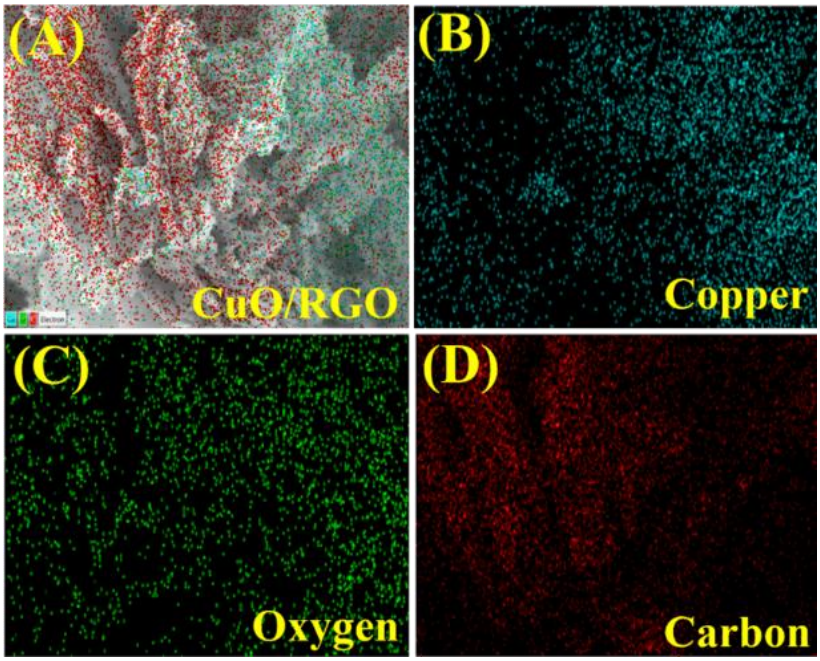

Fig. 5. Elemental mapping of CuO/RGO nanocomposites

In addition, Raman spectroscopy was performed to confirm the presence of GO, RGO in the CuO-RGO composites. Fig.6 (A-C) depicting the comparison of the Raman spectra of, GO, RGO, and CuO-RGO respectively. In the case of GO, there are two typical bands found at 1332.34 and 1581.73 cm^{-1}, which attributed to disordered sp^2 carbon (D band) and well-ordered graphite (G band), respectively. Compared with GO (ID/IG = 0.842), an increased D/G intensity ratio (ID/IG = 0.85) is observed in RGO (1363.72 and 1608.51 cm^{-1}), suggesting the reduction of GO to RGO. As for CuO-RGO composites, the sharp peak centred at about 1349.39 and 1603.45 cm^{-1} and the decreased intensity ratio (ID/IG = 0.841).

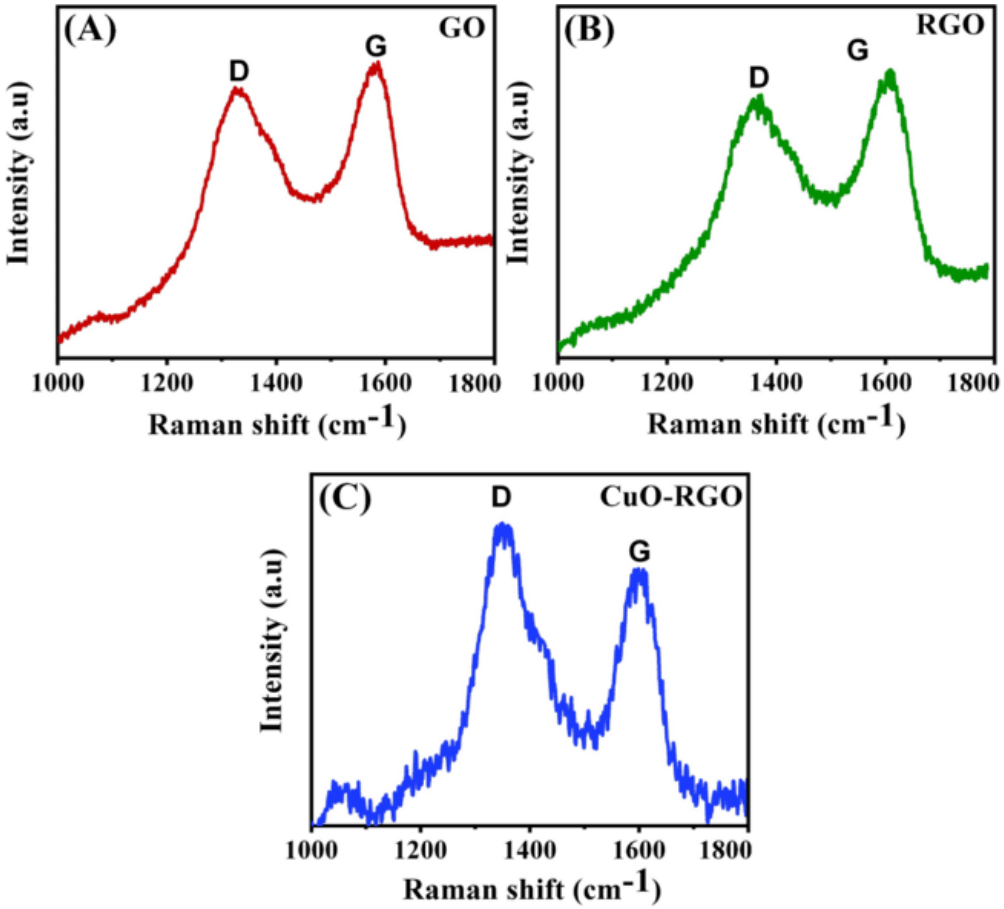

Fig. 6. Raman spectra of GO, RGO, and CuO/RGO nanocomposites

3. Electrochemical characterization studies (EIS)

Fig. 7 depicting the impedance spectra of each electrode fabrication step in addition to the morphological images and Randles equivalent circuit as inset. The electro catalytic behavior of each fabricated step was observed by EIS measurements in 5mM $[Fe(CN)6]^{-3/-4}$ in 0.1 M KCl solution, and the impedance result were obtained using Randle's equivalent circuit. The bare SPCE (curve (a)) displays the largest semicircle with the R_{et} of 1159.026 Ω. However, after CuO NPs growth on SPCE, the Nyquist semicircle becomes smaller and R_{et} value was decreased (R_{et} = ~113.16 Ω, (curve (b)), indicating the enhanced electron transfer rate. Then, RGO modified SPCE shows the improved electron transfer rate and the semicircle is smaller than the CuO/SPCE (Ret = ~93.408 Ω). To select the most suitable electrode, we modified the CuO NPs grown on SPCE with RGO after dipping CuO NPs/RGO/SPCE in the precursor solution. Afterwards, CuO modification, the CuO/RGO/SPCE shows improved electron transfer rate, compared with the other modified electrode. This modified electrode shows the enhanced electron transfer rate (curve d, R_{et} = ~28.263 Ω). The results proposed the controlled CuO modification over the RGO/SPCE is important, as less (curve (c)) and more (curve (e)) modification gives high electron transfer resistance. The lowest Ret reflects the limit of diffusion process occur between the electrode surface and the solution. Therefore, CuO/RGO nanocomposites was favored for further electrochemical descriptions and para-aminophenol detection.

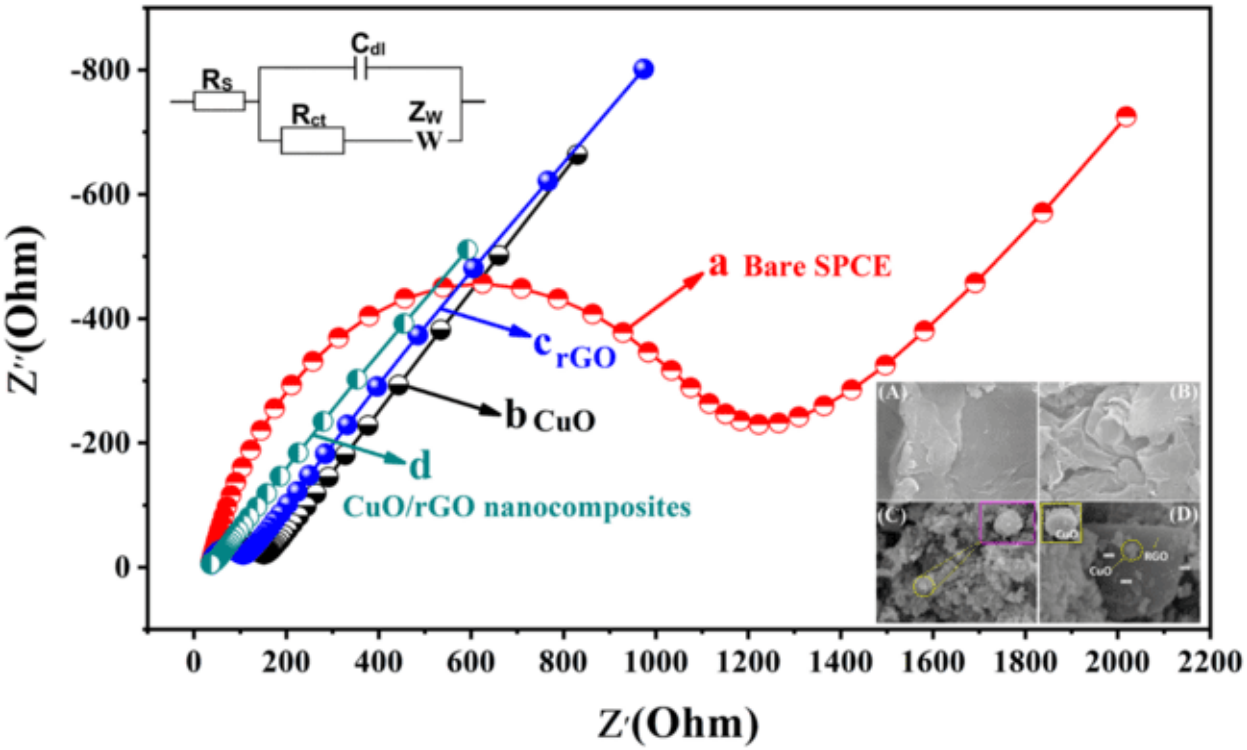

Fig. 7. Typical Cole-Cole plots for the EIS measurements at bare SPCE (a), RGO/SPCE (b), CuO/SPCE (c), and CuO/RGO/SPCE modified electrode (d) containing 1mM of $[Fe(CN)6]^{-3/-4}$ Inset shows the corresponding morphological images of the bare SPCE, CuO, RGO and CuO/RGO respectively. Randle equivalent circuit model employed for data fitting.

Table 1. Comparison of Ret values obtained at different modified electrode by EIS analysis.

Electrode type	Electron transfer resistance, R_{et} (Ohm)
Bare SPCE	1159
CuO/SPCE	113
RGO/SPCE	93
CuO/RGO/SPCE	28

6. Electro catalytic activity of PAP on CuO/RGO /SPCE

The electrochemical investigation provide a very adaptable means of kinetic, mechanistic and electro-synthesis studies. Electrochemical techniques are widely used to obtain thermodynamic and kinetic data about the reactions of inorganic and organic substances over a wide time window (sub-microseconds to hours). It is known the Cyclic voltammogram (CV) is a powerful tool for the investigation of electrochemical reactions that are coupled with chemical reactions occur at the surface of electrode. [45-53].

The electro catalytic behavior of PAP (200 µM) on bare SPCE, CuO/SPCE, RGO/SPCE, and CuO/RGO/SPCE were investigated in 0.05 M phosphate buffer supporting electrolyte (pH 7.0). The applied potential ranging from -0.2 to +0.6 V at a scan rate of 0.05 Vs^{-1} in Cyclic voltammogram under N_2 saturated condition (Fig. 8). In the presence of 200 µM of PAP for each electrode Fig. 8 (A), in the selected scanning portion for bare SPCE curve (a), a semi-reversible redox peaks were noticed and the anodic peak potential (E_{pa}) is 0.31035 V and the cathodic peak potential (E_{pc}) of 0.07016 V. Then, CuO/SPCE modified electrode shows the slightly improved an anodic and cathodic peak at the region of 0.2599 V and 0.0446 V (curve b). As shown in Fig. 8 (c) RGO/SPCE modified electrode exhibits the anodic and cathodic peaks in the region of E_{pa} = 0.2369 V and E_{pc} = 0.0344 Volts respectively. At CuO/RGO/SPCE (curve d), a pair of well-defined and a quasi-reversible redox peaks corresponding to the electrochemical reaction of PAP were observed with E_{pa} = 0.14585 V and E_{pc} = 0.09164 V. Compared with bare SPCE, CuO/SPCE, and RGO/SPCE, the CuO/RGO/SPCE modified electrode has shown better electro catalysis for PAP which is evident from the observed low ΔE_p (0.05425 V). The obtained redox peak current of PAP on the modified electrode was Due to the oxidation and reduction reaction with two electrons and two protons transfer process. Fig. 8A (curve (d)), shows a forward peak (curve (e)i)) for the positive going sweep and a reverse peak in the negative going sweep (curve (e)ii)). According to the previously published reports, [54-55] the observed catalytic behaviour of PAP is closely related to hydrolysis reaction of para-aminoquinoneimine (3_{ox}) as shown in **Scheme 2.** The potential peak current ratio for the peaks (i) and (ii) (I_{pc}/I_{pa}) deviates from unity and was reduced as a results of participation 3_{ox} in hydrolysis reaction under the experimental conditions, the cathodic peak could be relevant to the reduction of 1,4-benzoquinone. All these results suggest that CuO/RGO/SPCE is the suitable electrode with enhanced electro catalytic performance for PAP determination. Fig. 8 (B) depicts further Cyclic voltammetry response for CuO/RGO/SPCE with the continuous addition of PAP from 50 µM to 300 µM in 0.05M PBS (PH=7.0) at a scan rate 0.05Vs^{-1}. Fig. 8 (B) shows that the redox peak currents significantly increase with the increasing the concentration of 50µM to 300µM. To determine the limit of detection, selectivity and sensitivity, of the CuO/RGO/SPCE modified electrode was selected as the working electrode, and the oxidation peaks was used as the analytical signal in DPV Due to the current peaks obtained by this technique are better and sharper defined with a low background current and improved resolution compared to the Cyclic voltammetry (CV).

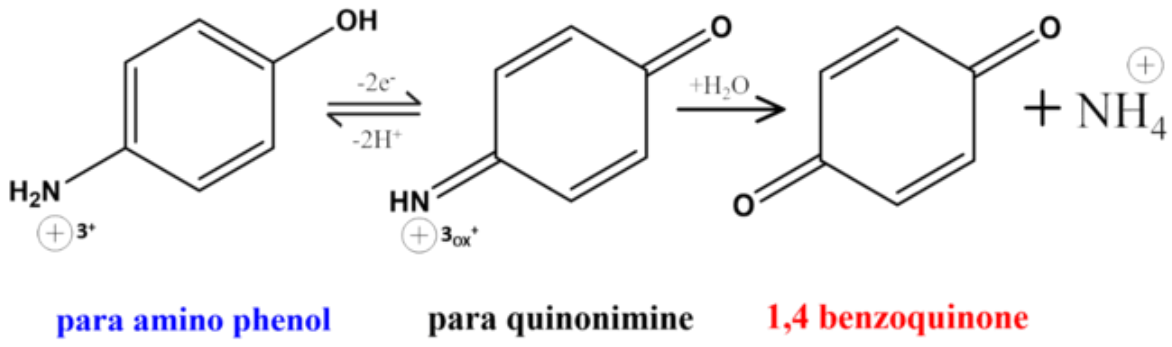

Scheme 2. Electrochemical oxidation mechanism of PAP at CuO/RGO/SPCE.

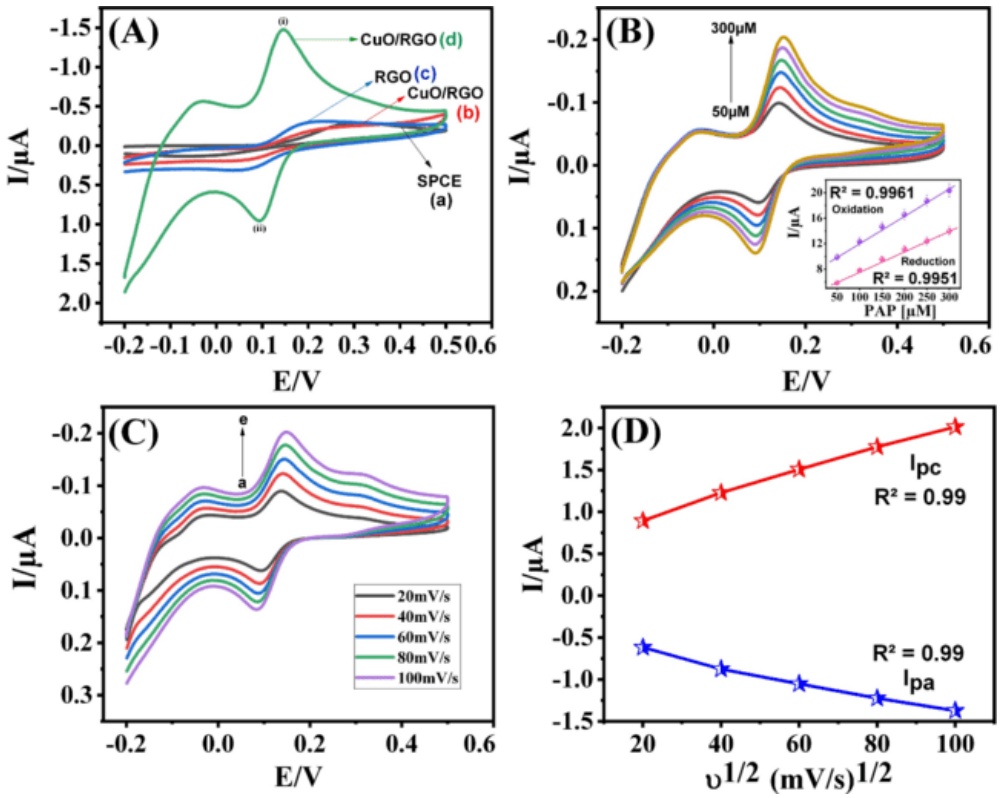

Fig. 8. The electrochemical response of the PAP sensing electrode. (A) Cyclic voltammetry response of the different modified electrode in 0.05 Mole PBS supporting electrolyte (pH -7.0) in the absence and presence of 200µM PAP recorded with the scan rate 0.05 Vs^{-1} in the potential ranging from -0.2 to +0.6 V. CVs of various additions of PAP (B). different potential scan rates and corresponding linear current plots (C) and (D).

6.1. Influence of scan rate

Taking into the electrochemical redox mechanism of PAP, the effect of scan rate (ν) on the voltammetry response at the modified electrode were studied in detail. Fig.8 (C) represents the Cyclic voltammograms of CuO/RGO/SPCE in the supporting electrolyte 0.05 M phosphate buffer (pH-7.0) containing 200 µM of PAP with the scan rate ranging from 20 to 100 mVs^{-1}. A good linear relationship between the peak current and the square root of the scan rate ($\nu^{1/2}$) from 20 to100 mVs^{-1} was obtained. The linear regression equations are shows in Fig.8 (D), which mentions that the redox of PAP at CuO/RGO/SPCE is a diffusion-controlled process and the corresponding equation could be expressed in the equations (4) and (5), from which the electrochemical redox mechanism takes place by the involvement of two electrons and two protons. The possible mechanism is depicted in **Scheme 3.**

$$I_{pa}/A = -0.0929x \text{ (scan rate)}^{1/2} - 4.7026 \ (R^2 = 0.99) \rightarrow (4)$$

$$I_{pc}/A = 0.1395x \text{ (scan rate)}^{1/2} + 6.4728 \ (R^2 = 0.99) \rightarrow (5)$$

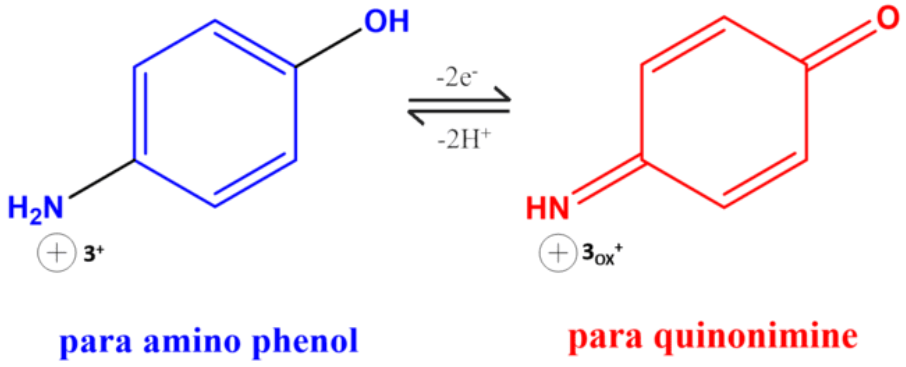

Scheme 3. Electron transfer mechanism of PAP on CuO/RGO/SPCE.

6.2. Differential pulse voltammetry analysis of PAP

To further improve the electro catalytic performance of CuO/RGO/SPCE for the determination PAP, the DPV was performed at the potential step from -0.2 to +0.6 V. The forward peak current response were observed for the PAP oxidation at different concentrations in the presence of CuO/RGO/SPCE modified electrode. Notably, the response of an anodic peak current increased linearly at the continuous addition of PAP from the ranging 0.01 µM to 478.1 µM shown in Fig. 9 (A) and Fig. 9 (B) shows the corresponding linear current calibration plots. The sequential regression equation was expressed as Ip(µA) = -0.1386x + 2.0485 [PAP]/µM; R^2= 0.9962. The detection limit (S/N=3) was calculated to be 0.0216 µM and the sensitivity of the electrode is 1.7544 mA $mM^{-1}cm^{-2}$. The limit of detection (LOD) values of experimentally resolved PAP and detailed LOD values are tabulated in **Table 2**. In comparison at the different modified electrode, the CuO/RGO/SPCE modified electrode provided a vast linear ranging for PAP determination and a low level of detection. Thus, all results suggest that the CuO/RGO/SPCE possesses the ability for the quantitative determination of PAP. The lower detection limit can be calculated by using the following equation (6);

$$\boldsymbol{LOD = \frac{3S_B}{b}} \qquad \rightarrow \qquad (6)$$

Where S_B is the standard deviation of the blank signal and b is the sensitivity.

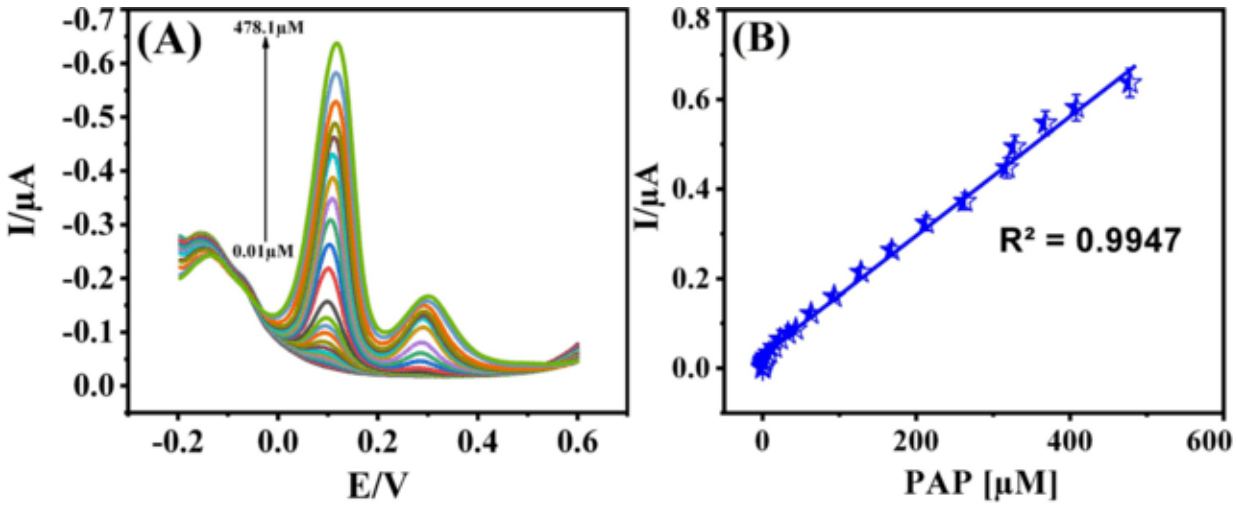

Fig. 9. (A) Differential pulse voltammograms for PAP sensor under the sequential addition of PAP at various concentrations in the presence of supporting electrolyte 0.05 M PBS (pH -7.0) at the potential scan rate 0.05 V/s^{-1}. (B) Linear current calibration plots.

Table 2. Comparison of an electrochemical sensor for PAP at different modified electrode.

Modified electrode	Methods	LOD (µM)	Linear ranging (µM)	Reference
Mesoporous silica modified [a]CPE	DPV	0.092	0.2-28	[56]
[b]PEDOT/GCE	DPV	1.2	4-320	[57]
[c]PBHQ	FOR	0.18	0.92-20	[58]
[d]SPCE	NPV	0.05	0.2-200	[59]
[e]SWCNT/POAPE	CV	0.06	0.2-100	[6]
[f]Hemin-modified MIP	AMP	3.00	10-90	[60]
MoS_2	DPV	0.03	0.04-17	[61]
[g]Graphene/Nafion/GCE	DPV	0.051	0.5-200	[62]
[h]CuO/RGO/SPCE	DPV	0.002	0.01-478.1	This work

[a]CPE: carbon paste electrode. [b]PEDOT: Poly (3, 4-ethylenedioxythiophene), [c]PBHQ: 2, 2-(1,4-Phenylenedivinylene) bis-8-hydroxyquinoline, [d]SPCE: screen printed carbon electrode, [e]SWCNT: single-walled carbon nanotubes, [f]MIP: molecular imprinted polymer, POAPE: Poly (4-aminopyridine), [g]GCE: glassy carbon electrode.

6.3. Specificity, Repeatability, Reproducibility and Storage Stability tests for PAP sensor

The anti-interference ability for the CuO/RGO/SPCE modified electrochemical sensor device for the determination for PAP is a key challenge, which could affect the performance of the electrode materials. The selectivity for CuO/RGO/SPCE was tested in the presence of various interferences such as paracetamol (PRT), amoxicillin (AMOX), chloramphenicol (CAP), tyrosine (TYR), 4-nitro phenol (4-NP), uric acid (UA), salicylic acid (SA), sodium sulphide (Na_2S) and glucose (GLU). The DPV response of the sensor was recorded at the addition of 50 µM for PAP and 30 µM each of the above interference substances in 0.05 M of phosphate buffer at the potential span from -0.2 to +0.6 V (*versus* Ag/AgCl), as shown in Fig.10 (A). The addition of 50 µM PAP resulted in the fast current response, whereas addition interferent substance shows no significant current response. An enhanced view of each interference addition and the current response is shows in the flowchart Fig.10 (B), which shows the current response compared to 50 µM for PAP. The results proved that the CuO/RGO/SPCE modified electrode for the selectively detect PAP in real time.

The feasibility, reproducibility, and storage stability analysis are another important criterion for quantifying the proficiency for the sensor. The repeatability for the CuO/RGO/SPCE

modified electrode were analyzed by five repeatable measurements and the obtained related standard deviation (RSD) was 1.7287%. To calculate the reproducibility for the sensor was analyzed at five different CuO/RGO/SPCE fabricated electrode and their DPV response to the 100 µM for PAP was monitored. The RSD values for five DPV measurements were 2.412%. The long-term storage stability for the modified sensor was tested by storing the modified electrode in a refrigerator at 4˚C for 20 days. Then, the sensor was employed to determine the freshly prepared PAP. The CV response was observed in the presence of 50 µM for PAP in 0.05 M phosphate buffer (pH-7.0) at the scanning time 0.05 V/s^{-1}. Hence, the fabricated sensor device shows excellent repeatability and reproducibility for the PAP determination.

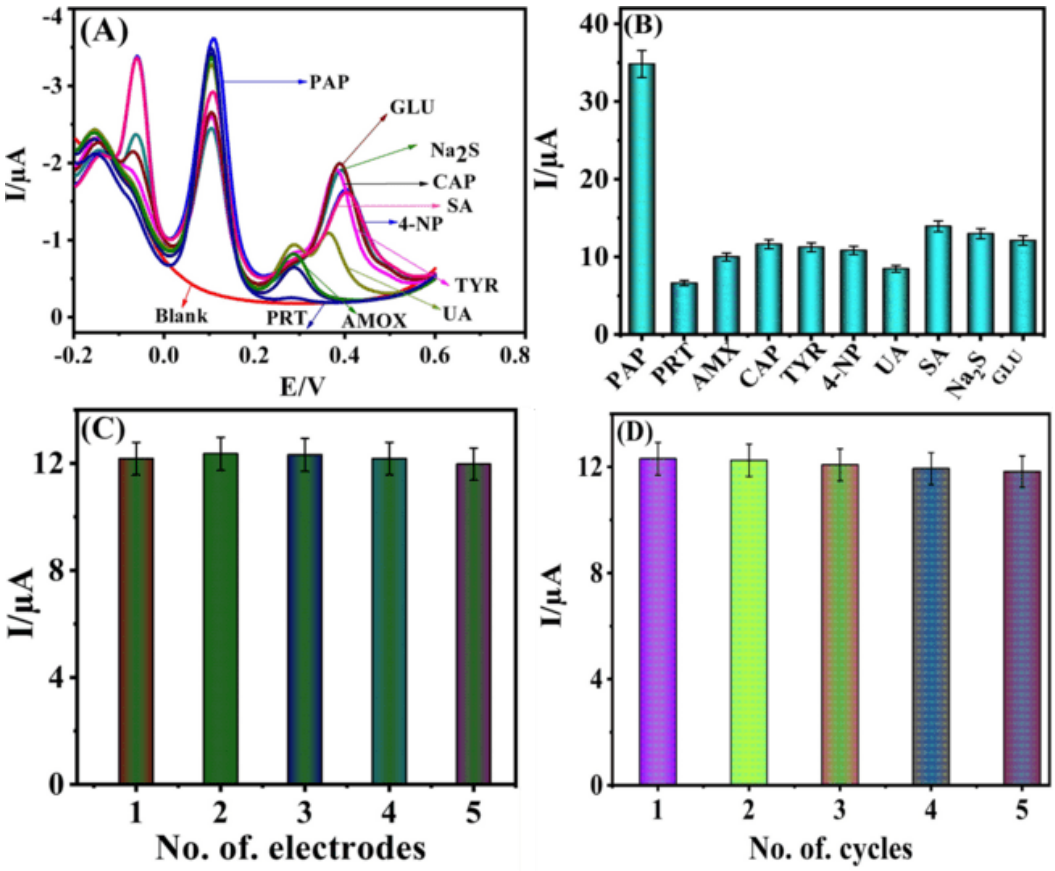

Fig. 10. Selectivity performance for CuO/RGO/SPCE modified electrodes. (A) Differential pulse voltammetry response for the sensor in 0.05 Mole PBS (pH- 7.0) under the potential steps between -0.2 to + 0.60 volts *versus* Ag/AgCl at the scan rate 50mV/s. (B) corresponding calibration for current plots. (C) And (D) Repeatability and Reproducibility current response for PAP sensing electrodes.

6.4. PAP determination in real samples

The sensing ability for CuO/RGO/SPCE modified electrode were tested to detect the PAP in real samples. We noted the DPV results for CuO/RGO/SPCE in 0.05 M phosphate buffer. Each of the experiments attained under the potential span from -0.2 to +0.60 V (*versus* Ag/AgCl). Water samples and wild berry fruit extract is filtered and spiked with known concentrations for PAP. In these cases, the good electrochemical response was observed, as summarized in **Table 3**. Therefore, the fabricated CuO/RGO/SPCE sensor may have the potential application for PAP determination in real water samples.

Table. 3 Electrochemical determination for PAP on CuO/RGO/SPCE modified electrode in a tap water samples.

Samples	Amount added (µM)	Amount Found (µM)[a]	Recovery (%)	RSD (%)[b]
Drinking water	0	-	-	-
	10	9.76	97.61	3.214
	20	20.21	101.05	2.92
	30	30.16	100.53	2.986
River water	0	-	-	-
	10	9.51	95.16	3.62
	20	19.82	99.14	3.182
	30	30.37	101.23	2.814
Wild Berry Fruit extract	0	-	-	-
	10	9.82	98.24	3.64
	20	20.17	100.85	4.69
	30	30.016	100.05	4.27

[a] standard addition method. [b] Relative standard deviation deuced from three separate measurements.

7. Conclusions

The present work illustrates the electrochemical behavior for para-aminophenol (PAP) on CuO/RGO modified screen-printed carbon electrode (SPCE). The suggest electrochemical sensor shows a good electro catalytic activity for the determination for PAP Due to the synergic effects for CuO/RGO nanocomposites, which are presented on the surface for the SPC electrodes. Moreover, the fabricated sensor was applied successfully for the quantification for PAP in the environmental samples.

Conflicts of Interest

"There are no conflicts to declare".

Notes and References

[1] NG. Karousos, SM. Reddy "Determination of 4-aminophenol using the quartz crystal microbalance sensor." Analyst 127, no. 3 (2002): 368-372.

[2] C. V. Rode, M. J. Vaidya, R. Jaganathan, and R. V. Chaudhari, Hydrogenation of nitrobenzene to p-aminophenol in a four-phase reactor: reaction kinetics and mass transfer effects. Chem. Engi. Sci., 56 (2001), 1299-1304.

[3] Y. Lia, C. M. Bentzleyb, and J. B. Tarloffa, Comparison of para-aminophenol cytotoxicity in rat renal epithelial cells and hepatocytes. Toxicology, 209, (2005), 69-76.

[4] Q. Chu, L. Jiang, X. Tian, and J. Ye, Rapid determination of acetaminophen and p-aminophenol in pharmaceutical formulations using miniaturized capillary electrophoresis with amperometric detection. Anal. Chim. acta, 606, (2008), 246-251.

[5] M.B. Jacobs. “Analytical chemistry of industrial poisons, hazards, and solvents." In Analytical chemistry and its applications, vol. 1. Elving & Kolthoff, 1949.

[6] R. C. Russo. "Development of marine water quality criteria for the USA." Mar. Pollut. Bull 45, no. 1-12 (2002): 84-91.

[7] Z. Wang, H. Zhu, H. Zhang, G. Gao, Z. Sun, H. Liu, X. Zhao. "Fabrication of the single-wall carbon nanotube compound polymer film electrode and the simultaneous electrochemical behavior of aminophenol isomers." Electrochim Acta 54, no. 28 (2009): 7531-7535.

[8] A. Yesilada., H. Erdogan, M. Ertan. "Second derivative spectrophotometric determination of p-aminophenol in the presence of paracetamol." Anal. lett 24, no. 1 (1991): 129-138.

[9] G. López-Cueto, S. Maspoch, JF. Rodríguez-Medina, C. Ubide. "Simultaneous kinetic spectrophotometric determination of o-, and p-aminophenol using partial least squares calibration." Analyst 121, no. 4 (1996): 407-412.

[10] K. S. Novoselov, A. K. Geim. "The rise of graphene." Nat. Mater 6, no. 3 (2007): 183-191.

[11] K. S. Novoselov, A. K. Geim, Sergei V. Morozov, D. Jiang, Y_ Zhang, Sergey V. Dubonos, Irina V. Grigorieva, and Alexandr A. Firsov. "Electric field effect in atomically thin carbon films." Science 306, no. 5696 (2004): 666-669.

[12] S. Stankovich., D. A. Dikin, G.H. Dommett, K.M. Kohlhaas, K.M., Zimney, E.J., Stach, E.A., Piner, R.D., S.T. Nguyen, R.S. Ruoff,"Graphene-based composite materials." Nature 442, no. 7100 (2006): 282.

[13] X. Wang, L. Zhi, K. Müllen, "Transparent, conductive graphene electrodes for dye-sensitized solar cells." Nano Lett 8, no. 1 (2008): 323-327.

[14] J.T. Robinson, F.K Perkins, E.S. Snow, Z. Wei, P.E. Sheehan. "Reduced graphene oxide molecular sensors." Nano Lett 8, no. 10 (2008): 3137-3140.

[15] Z. Liu, T. Robinson, X. Sun, H. Dai. "PEGylated nanographene oxide for delivery of water-insoluble cancer drugs." J. Am. Chem. Soc 130, no. 33 (2008): 10876-10877.

[16] M.D. Stoller, S. Park, Y. Zhu, J. An, R.S. Ruoff. "Graphene-based ultracapacitors." Nano Lett 8, no. 10 (2008): 3498-3502.

[17] M.J. Allen, V.C. Tung, R.B. Kaner, "Honeycomb carbon: a review of graphene." Chem. Rev 110, no. 1 (2009): 132-145.

[18] S. Park, J. An, J.R. Potts, A. Velamakanni, S. Murali, R.S. Ruoff. "Hydrazine-reduction of graphite-and graphene oxide." Carbon 49, no. 9 (2011): 3019-3023.

[19] Y. Hernandez, V. Nicolosi, M. Lotya, F.M. Blighe, Z. Sun, S. De, I.T. McGovern, B. Holland, M. Byrne, Y.K. Gun'Ko, J.J. Boland. High-yield production of graphene by liquid-phase exfoliation of graphite. Nat. Nanotechnol.3 (2008): 563.

[20] H.J. Park, J. Meyer, S. Roth, V. Skákalová. "Growth and properties of few-layer graphene prepared by chemical vapor deposition." Carbon 48, no. 4 (2010): 1088-1094.

[21] G.M. Scheuermann, L. Rumi, P. Steurer, W. Bannwarth, R. Mülhaupt. "Palladium nanoparticles on graphite oxide and its functionalized graphene derivatives as highly active catalysts for the Suzuki−Miyaura coupling reaction." J. Am. Chem. Soc 131, no. 23 (2009): 8262-8270.

[22] S. Guo, D. Wen, Y. Zhai, S. Dong, E. Wang. "Platinum nanoparticle ensemble-on-graphene hybrid nanosheets: one-pot, rapid synthesis, and used as new electrode material for electrochemical sensing." ACS Nano 4, no. 7 (2010): 3959-3968.

[23] R. Muszynski, B. Seger, P.V. Kamat. "Decorating graphene sheets with gold nanoparticles." J. Phys. Chem. C 112, no. 14 (2008): 5263-5266.

[24] K.K. Manga, S. Wang, M. Jaiswal, Q. Bao, K.P. Loh, "High-Gain Graphene-Titanium Oxide Photoconductor Made from Inkjet Printable Ionic Solution." Adv. Mater 22, no. 46 (2010): 5265-5270.

[25] B. Li, H. Cao, J. Shao, M. Qu, J.H. Warner. "Superparamagnetic Fe_3O_4 nanocrystals@ graphene composites for energy storage devices." J. Mater. Chem 21, no. 13 (2011): 5069-5075.

[26] B. Li, H. Cao, G. Yin, "$Mg(OH)_2$@ reduced graphene oxide composite for removal of dyes from water." J. Mater. Chem 21, no. 36 (2011): 13765-13768.

[27] B. Li, H. Cao, "ZnO@ graphene composite with enhanced performance for the removal of dye from water." J. Mater. Chem 21, no. 10 (2011): 3346-3349.

[28] J. S. Shaikh, R. C. Pawar, A. V. Moholkar, J. H. Kim, and P. S. Patil. "CuO–PAA hybrid films: chemical synthesis and supercapacitor behavior." Appl. Surf. Sci 257, no. 9 (2011): 4389-4397.

[29] H. Zhang, M. Zhang. "Synthesis of CuO nanocrystalline and their application as electrode materials for capacitors." Mater. Chem. Phys 108, no. 2-3 (2008): 184-187.

[30] J.E. Jeronsia, D.V. Raj, L.A. Joseph, K. Rubini, S.J. Das. "In vitro antibacterial and anticancer activity of copper oxide nanostructures in human breast cancer Michigan Cancer Foundation-7 cells." J. Med. Sci 36, no. 4 (2016): 145.

[31] A. El-Trass, H. ElShamy, I. El-Mehasseb, M. El-Kemary. "CuO nanoparticles: synthesis, characterization, optical properties and interaction with amino acids." Appl. Surf. Sci 258, no. 7 (2012): 2997-3001.

[32] X. Jia, H. Fan, W. Yang. "Hydrothermal synthesis and primary gas sensing properties of CuO nanosheets." J. Dispersion. Sci. Technol 31, no. 7 (2010): 866-869.

[33] J.E. Jeronsia, DJ. Vidhya Raj, L. Allwin Joseph, K. Rubini, S. Jerome Das. "In vitro antibacterial and anticancer activity of copper oxide nanostructures in human breast cancer Michigan Cancer Foundation-7 cells." J. Med. Sci 36, no. 4 (2016): 145.

[34] D. Das, B.C. Nath, P. Phukon, S.K. Dolui, "Synthesis and evaluation of antioxidant and antibacterial behavior of CuO nanoparticles." Colloids. Surf. B: Bio-interfaces 101 (2013): 430-433.

[35] C.Y. Chiang, K. Aroh, N. Franson, V.R. Satsangi, S. Dass, S. Ehrman, "Copper oxide nanoparticle made by flame spray pyrolysis for photoelectrochemical water splitting–Part I. CuO nanoparticle preparation." Int. J. Hydrog. Energy 37, no. 6 (2012): 4871-4879.

[36] Z. Zhao, M. Zhang, X. Chen, Y. Li, J. Wang. "Electrochemical co-reduction synthesis of AuPt bimetallic nanoparticles-graphene nanocomposites for selective detection of dopamine in the presence of ascorbic acid and uric acid." Sensors 15, no. 7 (2015): 16614-16631.

[37] K. Jackowska, P. Krysinski, "New trends in the electrochemical sensing of dopamine." Anal. Bioanal. Chem 405, no. 11 (2013): 3753-3771.

[38] W. Jia, E. Reitz, P. Shimpi, E.G Rodriguez, P.X. Gao, Y. Lei, Spherical CuO synthesized by a simple hydrothermal reaction: concentration-dependent size and its electro catalytic application. MRS. Bull 44, 8, (2009). pp.1681-1686.

[39] E. Shahsavani, N. Feizi, A. Dehno Khalaji. "Copper oxide nanoparticles prepared by solid state thermal decomposition: synthesis and characterization." Journal of Ultrafine Grained and Nanostructured Materials 49, no. 1 (2016): 48-50.

[40] Y. Liu, W. Wang, L. Gu, Y. Wang, Y. Ying, Y. Mao, L. Sun, X. Peng. "Flexible CuO nanosheets/reduced-graphene oxide composite paper: binder-free anode for high-performance lithium-ion batteries." ACS Appl. Mater. Interfaces 5, no. 19 (2013): 9850-9855.

[41] B. Zhao, P. Liu, H. Zhuang, Z. Jiao, T. Fang, W. Xu, B. Lu, Y. Jiang. "Hierarchical self-assembly of microscale leaf-like CuO on graphene sheets for high-performance electrochemical capacitors." J. Mater. Chem A 1, no. 2 (2013): 367-373.

[42] B. Wang, X.L. Wu, C.Y. Shu, Y.G. Guo, C.R. Wang, "Synthesis of CuO/graphene nanocomposites as a high-performance anode material for lithium-ion batteries." J. Mater. Chem 20, no. 47 (2010): 10661-10664.

[43] W.S. Hummers Jr, R.E. Offeman, "Preparation of graphitic oxide." J. Am. Chem. Soc 80, no. 6 (1958): 1339-1339.

[44] P.S. Kumar, M. Selvakumar, S.G. Babu, S. Karuthapandian, S. Chattopadhyay. "CdO nanospheres: facile synthesis and bandgap modification for the superior photocatalytic activity." Mater. Lett 151 (2015): 45-48.

[45] C. Costentin, Electrochemical approach to the mechanistic study of proton-coupled electron transfer. Chem. Rev, 108, (2008), 2145-2179.

[46] F. Varmaghani, D. Nematollahi, S. Mallakpour, and R. Esmaili, Electrochemical oxidation of 4-substituted urazoles in the presence of arylsulfinic acids: an efficient method for the synthesis of new sulfonamide derivatives. Green Chem., 14, (2012), 963-967.

[47] A. Houmam, 2008. Electron transfer initiated reactions: Bond formation and bond dissociation. Chem. Rev., 108, (2008), 2180-2237.

[48] R. Esmaili and D. Nematollahi, Electrochemical oxidation of 4-morpholinoaniline in aqueous solutions: Synthesis of a new trimer of 4-morpholinoaniline. Electrochim. Acta, 56, (2011), 3899-3904.

[49] H. Shayani-Jam and D. Nematollahi. "Electrochemical evidences in oxidation of acetaminophen in the presence of glutathione and N-acetylcysteine." Chem. Commun, 46, no. 3 (2010), 409-411.

[50] D. Nematollahi and F. Varmaghani. "Paired electrochemical synthesis of new organosulfone derivatives." Electrochim. Acta, 53, no. 8 (2008): 3350-3355.

[51] A. Maleki and D. Nematollahi. "An efficient electrochemical method for the synthesis of methylene blue." Electrochem. Commun, 11, no. 12 (2009): 2261-2264.

[52] A. J. Bard and L. R. Faulker. "Fundamentals and applications." Electrochemical Methods 2nd ed., Wiley, New York, (2001): 482.

[53] R. Greef, R. Peat, L. M. Peter, D. Pletcher, and J. Robinson, Instrumental Methods in Electrochemistry, Ellis Horwood Limited, New York, (1990), 443, doi:10.1002/bbpc.19860900614.

[54] H. J. Salavagione, J. Arias, P. Garces, E. Morallon, C. Barbero, and J. L. Vazquez. Spectroelectrochemical study of the oxidation of aminophenols on platinum electrode in acid medium. J. Electroanal. Chem, 565, (2004), 375-383.

[55] Y. Song. Theoretical studies on electrochemistry of p-aminophenol. Spectrochim. Acta, Part A., Molecular and Biomolecular Spectroscopy, 67, (2007), 611-618.

[56] D. Sun, X. Li, H. Zhang, X. Xie. "An electrochemical sensor for p-aminophenol based on the mesoporous silica modified carbon paste electrode." Int. J. Environ. Anal. Chem 92, no. 3 (2012): 324-333.

[57] S. Mehretie, S. Admassie, T. Hunde, M. Tessema, T. Solomon. "Simultaneous determination of N-acetyl-p-aminophenol and p-aminophenol with poly (3, 4-ethylenedioxythiophene) modified glassy carbon electrode." Talanta 85, no. 3 (2011): 1376-1382.

[58] H. Filik, M. Hayvalı, E. Kılıç, R. Apak, D. Aksu, Z. Yanaz, T. Çengel, "Development of an optical fibre reflectance sensor for p-aminophenol detection based on immobilized bis-8-hydroxyquinoline." Talanta 77, no. 1 (2008): 103-109.

[59] W.Y. Su, S.M. Wang, S.H. Cheng. "Electrochemically pretreated screen-printed carbon electrodes for the simultaneous determination of aminophenol isomers." J. Electroanal. Chem 651, no. 2 (2011): 166-172.

[60] J.D.R.M. Neto, W.D.J.R. Santos, P.R. Lima, S.M.C.N. Tanaka, A.A. Tanaka, L.T. Kubota. "A hemin-based molecularly imprinted polymer (MIP) grafted onto a glassy carbon electrode as a selective sensor for 4-aminophenol amperometric." Sens. Actuators B: Chemical 152, no. 2 (2011): 220-225.

[61] J.V. Kumar, R. Karthik, S.M. Chen, K. Saravanakumar, M. Govindasamy, V. Muthuraj. "Novel hydrothermal synthesis of MoS_2 nanocluster structure for sensitive electrochemical detection of human and environmental hazardous pollutant 4-aminophenol." RSC Adv 6, no. 46 (2016): 40399-40407.

[62] H. Filik, G. Çetintaş, S.N. Koç, H. Gülce, and İ. Boz. Nafion-graphene composite film modified glassy carbon electrode for voltammetric determination of p-aminophenol. Russian Journal of Electrochemistry, 50, (2014), 243-252.

[63] K. Palpandi, K. Eswaran, B. Kavitha, R. Karthiga, M. Rajarajan and A. Suganthi, Novel Sphere CuO/Ag3PO4 Nanocomposites with Enhanced Visible Light Photocatalytic Activity for Degradation of Amaranth.

[64] K.Y. Hwa, P. Karuppaiah, N.S.K. Gowthaman, V. Balakumar, S. Shankar, and H.N Lim, 2019. Ultrasonic synthesis of CuO nanoflakes: A robust electrochemical scaffold for the sensitive detection of phenolic hazard in water and pharmaceutical samples. Ultrasonics sonochemistry, 58, p.104649.

[65] K. Palpandi, Facile Synthesis and Characterization of Nanowire-like Copper Oxide Electrodes for Sensitive Electrochemical Sensing of Paracetamol, DOI: https://doi.org/10.5281/zenodo.15643177 (2025).